Earth and Planetary Science Letters 619 (2023) 118306

Contents lists available at ScienceDirect

Earth and Planetary Science Letters

journal homepage: www.elsevier.com/locate/epsl

Release of mercury during contact metamorphism of shale: Implications for understanding the impacts of large igneous province volcanism

Henrik H. Svensen [a,*], Morgan T. Jones [a], Lawrence M.E. Percival [b], Stephen E. Grasby [c], Tamsin A. Mather [d]

[a] Department of Geosciences, Sem Sælands vei 1, 0371 Oslo, Norway
[b] Analytical, Environmental and Geochemistry Group (AMGC), Vrije Universiteit Brussel, Pleinlaan 2, 1050 Brussels, Belgium
[c] Natural Resources Canada - Geological Survey of Canada, 3303 33rd Street NW, Calgary, AB T2L 2A7, Canada
[d] Department of Earth Sciences, University of Oxford, South Parks Road, Oxford, OX1 3AN, UK

ARTICLE INFO

Article history:
Received 3 January 2023
Received in revised form 29 June 2023
Accepted 7 July 2023
Available online 26 July 2023
Editor: L. Coogan

Keywords:
large igneous province
sub-volcanic
sedimentary basin
contact metamorphism
mercury
thermogenic

ABSTRACT

Elevated mercury (Hg) in sedimentary strata are a widely used tracer for assessing the relationship between large igneous province (LIP) activity and global environmental change. A key unknown in applying this proxy is the extent to which Hg was sourced from contact metamorphism of sedimentary rocks during sill intrusions versus gaseous emissions of the magmas themselves. Here, we investigate Hg behaviour during contact metamorphism of shales. We show loss of 80–99% of the sedimentary Hg in contact aureoles in four case studies covering the interactions around dykes, sills and plutons associated the High Arctic LIP (Sverdrup Basin, Canada), the Karoo LIP (South Africa) and the Skagerrak-centred LIP (Oslo Rift, Norway). A combination of geochemical data and thermal modelling around a dyke from the High Arctic LIP shows 33% Hg volatilization in the aureole at 265–300 °C. The other cases show similar behaviours with significant lowering of organic-bound Hg, more significantly in the innermost 60% of the contact aureoles. We hypothesize that gaseous Hg is transported out of aureoles during metamorphism, together with CH_4 and CO_2. Furthermore, we estimate the thermogenic Hg mobilization from Karoo LIP aureoles as 72–192 t per km^3 of aureole, which is between 1–3 times the estimated volumetric Hg release from Karoo magmas. When scaling our results to the size of the shale portions of the Karoo Basin affected by the LIP and a timescale of 100 kyr of sill emplacement, the average Hg flux is calculated to have been 78–207 t/y with maximum values up to ~300 t/y. The pulsed nature of intrusive volcanism suggests that this thermogenic Hg flux could have dominated LIP Hg emissions during periods of their life span. Our results demonstrate that the global Hg cycle can be significantly perturbed following LIP-scale sill emplacement into organic-rich sedimentary rocks and our quantification of the emissions based on source-rock analysis provides important information for independent interpretation of the sedimentary Hg record.

1. Introduction

There is a broad temporal correlation between the emplacement of large igneous provinces (LIPs) and environmental changes in the geological record, particularly for the last 300 million years (e.g., Courtillot and Renne, 2003). These changes include carbon cycle perturbations, global climate change, widespread marine anoxia, seawater acidification, ozone layer depletion, and mass extinctions of flora and fauna in terrestrial and marine ecosystems (e.g., Bond and Grasby, 2017). Nonetheless, the nature of any causal relationship between LIPs and environmental crises remains debated in the scientific community, in part because of the multiple processes occurring simultaneously that may result in similar proxy signals. There are several potential mechanisms by which LIPs could have affected surface processes and environment (e.g., Jones et al., 2016). Subaerial volcanic degassing can lead to cooling through sulfur emissions and global warming through carbon emissions (Caldeira and Rampino, 1990). However, atmospheric lifetimes of sulfur are typically days in the troposphere and only a few years in the stratosphere, leading to uncertainty regarding

* Corresponding author.
E-mail address: hensven@geo.uio.no (H.H. Svensen).

https://doi.org/10.1016/j.epsl.2023.118306

whether sulfur emissions can sustain climate cooling over millennia (Schmidt et al., 2015). Alternatively, LIP carbon emissions could have driven long-term climate warming on a global scale, as carbon dioxide has a much longer atmospheric residence time than sulfate aerosols. Submarine LIPs, such as the Greater Ontong Java Plateau, are also thought to have had a considerable impact on Earth's climate and environment, and have been suggested as triggers for oceanic anoxic events following igneous submarine CO_2 degassing (e.g., Larson and Erba, 1999; Snow et al., 2005).

It is increasingly recognized that the volatile release from LIPs related to contact metamorphism of sedimentary rocks intruded by igneous plumbing systems may play an important role in mediating potential environmental impacts (e.g., Svensen et al., 2004, 2007; Heimdal et al., 2020). Sedimentary rocks are major reservoirs of environmentally important elements that may be volatilised and released to the atmosphere when subjected to high temperatures during these metamorphic processes. Several LIPs are associated with large, tabular sill and dyke complexes emplaced into sedimentary basins, leading to a wide range of metamorphic and hydrothermal effects, including the generation and venting of thermogenic gases (e.g., Svensen et al., 2004). Thus, the formation of LIPs in sedimentary basins can affect $>10^6$ km^3 of organic-, carbonate- and evaporite-bearing strata and result in metamorphic reactions, volatile loss, and transfer of components such as CO_2, CH_4, CO, CH_3Cl, SO_2, and Hg out of the contact aureoles (e.g., Aarnes et al., 2010; Shen et al., 2022; Yallup et al., 2013). Contact metamorphism has been cited as a key mechanism during LIP emplacements for driving rapid environmental change during events including the Paleocene-Eocene thermal maximum (PETM), the end-Permian and end-Triassic mass extinctions, and the Toarcian and Early Aptian oceanic anoxic events, helping to explain the varying environmental impacts of different LIPs (e.g., Svensen et al., 2004, 2009; Ganino and Arndt, 2009; Grasby et al., 2011; Aarnes et al., 2011b; Black et al., 2014).

Proxies for LIP activity in stratigraphic archives of major environmental change are currently sparse. Volcanic tephra layers are extremely useful for stratigraphic and chronological correlations, but they are geographically limited in extent, only significantly generated by explosive volcanism (whereas LIP-style eruptions were likely predominantly effusive) and are typically restricted to regions that were relatively proximal to the source volcanoes (e.g., Black et al., 2021). By comparison, present-day volcanism is one of the main natural sources of atmospheric Hg, which can be transported over large distances due to its primary emission as gaseous Hg^0 (Pyle and Mather, 2003; Bagnato et al., 2007). Recently, Hg anomalies have been proposed as a robust proxy for LIP activity in contemporaneous sedimentary rocks (Sanei et al., 2012; Grasby et al., 2019; Percival et al., 2021), with Hg concentrations typically normalized to the total organic carbon (TOC) content to correct for variations in the rate of organic matter deposition and preservation, a key host phase. Diagenetic processes, weathering and redox variability can also lead to changes in Hg concentrations and/or anomalies in the Hg/TOC ratios in sedimentary strata (e.g., Charbonnier et al., 2020; Park et al., 2022; Frieling et al., 2023). In certain depositional environments, sulphide and/or clay minerals can also act as important host phases of mercury in addition to organic material (e.g., Grasby et al., 2017; Shen et al., 2019, 2020). Nonetheless, there is much evidence that, although not the exclusive cause, Hg enrichment is often related to prolonged large-scale volcanic activity, at least for some LIPs (e.g., Grasby et al., 2019; Percival et al., 2021).

Sedimentary rocks containing organic matter represent a large crustal reservoir of Hg. Mudstones, shales, and coal generally contain 10–500 ppb Hg (cf. Grasby et al., 2019; Zaputlyaeva et al., 2020). Generation and migration of oil and gas is an additional and potentially important, but poorly understood, part of the Hg cycle (Liu et al., 2022). Source rock maturation leads to Hg enrichment in the oil and gas phase, and coal maturation produces Hg-rich gas (e.g., Guo et al., 2018).

Thermogenic degassing from contact metamorphism is a potentially significant further source of Hg during LIP emplacement in sedimentary basins. This assumption is based on contact aureole studies documenting a considerable lowering of bulk rock TOC during progressive metamorphism (cf. Aarnes et al., 2010), and the observation in other studies that Hg is associated with sedimentary organic matter (see Grasby et al., 2019, and references therein). Furthermore, even during diagenesis and volatile-generation from kerogen, a recent study shows that Hg is enriched in liquid phase (bitumen), making it likely that such a trend persists to higher temperatures and complete organic matter devolatilization (Zaputlyaeva et al., 2020). The timescale of contact metamorphic devolatilization is geologically very short (10's to 1000's of years) and may lead to rapid pore pressure-buildup, extensive fluid flow, and degassing to the surface via explosive pipe-like conduits (e.g., Svensen et al., 2004; Aarnes et al., 2012). For these reasons, contact metamorphism may be an important part of the global Hg cycle during LIP volcanism when it is emplaced in organic-rich rocks (e.g., Sanei et al., 2012; Shen et al., 2022). It has therefore been hypothesised that Hg is mobilized from the heated sedimentary rocks in contact aureoles and emitted to the surface via hydrothermal vent complexes. This mechanism represents a different geological model for Hg mobilization and sedimentary anomalies compared to that of primarily mantle-sourced Hg emitted during volcanic eruptions. While this possibility has been suggested in several studies of Hg/TOC stratigraphy (e.g., Sanei et al., 2012; Percival et al., 2015; Jones et al., 2019; Shen et al., 2019, 2022), the possibility of a contact metamorphic LIP-related Hg flux has had only limited direct study (Liu et al., 2022), and has not been tested through investigation of the aureoles associated with LIPs themselves.

The aim of this study is to understand the behaviour of Hg during the contact metamorphism associated with LIPs and to assess the importance of this process in the global Hg cycle. Our approach is based on measurements of contact aureoles around two sills, a dyke, and a pluton from three LIPs. We focus on the carbon and Hg concentrations, combined with thermal modelling of the aureoles around the intrusive igneous units.

2. Geological settings and contact aureoles

We present data from aureole outcrops related to a pluton in the Oslo Rift (Norway), three boreholes from the Karoo Basin (South Africa), and a dyke outcrop in the Sverdrup Basin (Canada). The Oslo Rift is part of the Skagerrak-centred LIP (SCLIP), which was marked by widespread intrusive and volcanic activity across Northern and Central Europe between 305 Ma and 260 Ma (e.g., Heeremans et al., 2004). Carbon isotope anomalies near the Carboniferous-Permian boundary may be related to the initial SCLIP activity (Wu et al., 2021). The Karoo Basin contains a large volume of dolerite sills and dykes emplaced as part of the Karoo-Ferrar LIP at around 183 Ma (e.g., Duncan et al., 1997), which likely contributed to climate and environmental changes during the Toarcian Stage (e.g., McElwain et al., 2005; Svensen et al., 2007; Heimdal et al., 2021). The Sverdrup Basin was affected by the igneous activity of the Cretaceous High Arctic LIP (HALIP) around 135–90 Ma, potentially contributing to the Early Aptian Oceanic Anoxic Event (Polteau et al., 2016).

2.1. Pluton-related contact metamorphism in the Oslo Rift

The Oslo Rift (Fig. 1A) initiated around 300 Ma and resulted in several stages of volcanic and igneous activity through the shallow

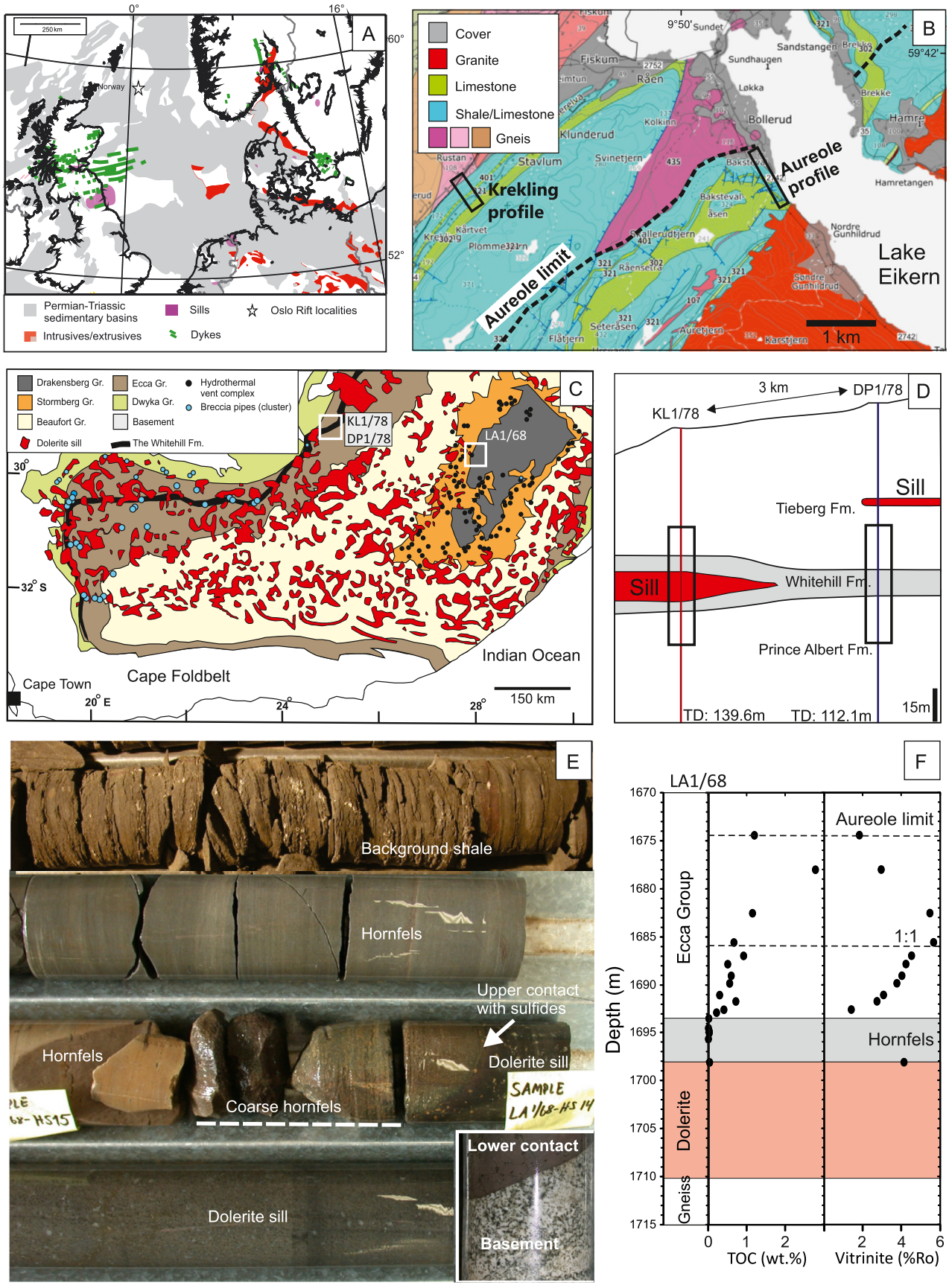

Fig. 1. A) Overview of volcanic activity around the Cretaceous-Permian boundary in Northern Europe, showing the location of the Oslo Rift. Modified from Heeremans et al. (2004). **B**) Geological map of the Gunhildrød contact aureole and the reference section for Cambrian shale at Krekling. **C**) Simplified geological map of the Karoo Basin showing the locations of the studied boreholes. **D**) Cross section showing the main divisions in the KL1/78 and DP1/78 boreholes. **E**) Core images from the lowermost sill and contact aureole in LA1/68. **F**) Published data from the lowermost contact aureole in LA1/68. From Svensen et al. (2015).

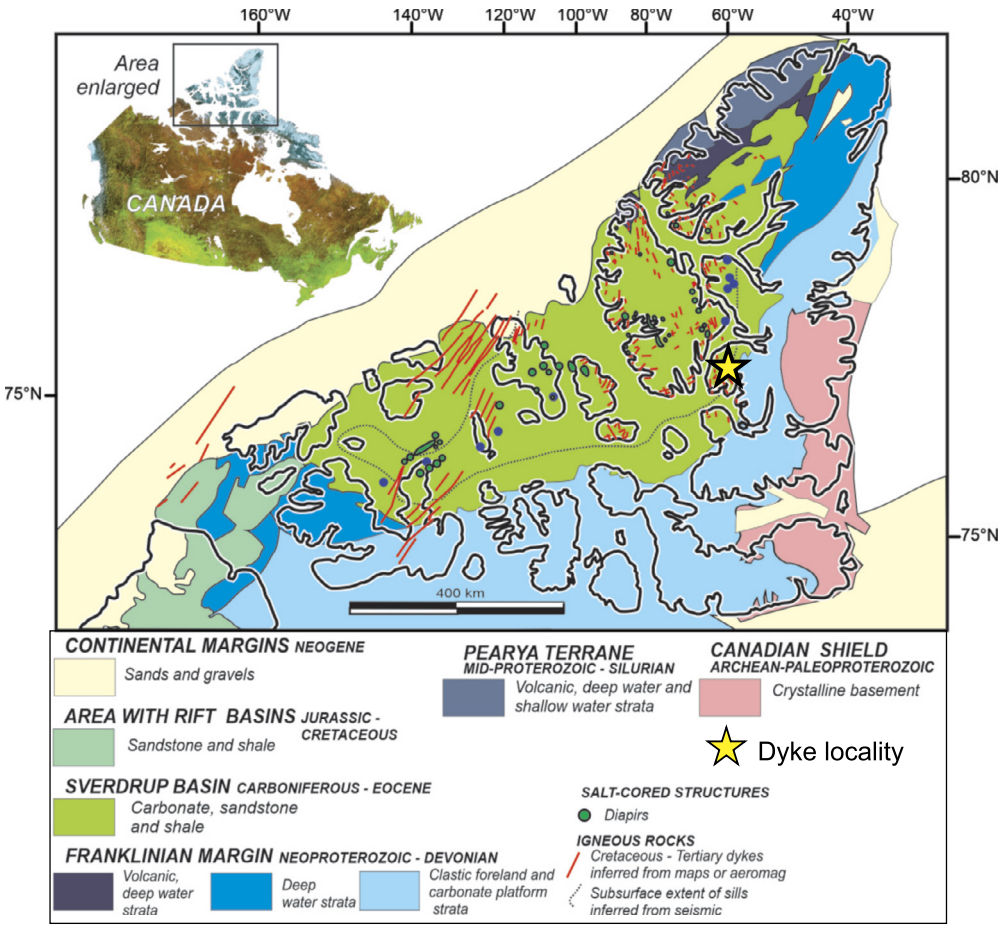

Fig. 2. Simplified geological map of the Sverdrup Basin with surrounding areas. We from data from a contact aureole with location (Axel Heiberg Island, Canada) shown by the star symbol.

crust with Cambrian to Silurian sedimentary rocks (e.g., Heeremans et al., 2004). Pluton emplacement resulted in kilometre-scale contact aureoles in surrounding shales and carbonates, giving rise to devolatilization, fluid flow, and late stage hydrothermal activity (e.g., Jamtveit et al., 1992). We sampled a transect through Cambrian black shale, about 800 m outwards from the contact with a Permian granite pluton at Gunhildrud, Eikern (Fig. 1B). We compare the aureole rocks (Hg, TOC, S) with sedimentary samples from a nearby and stratigraphically equivalent Cambrian shale at Krekling that was comparatively unaffected by the pluton (Hammer and Svensen, 2017). In the unaffected sedimentary rocks, the highest TOC contents reach almost 14 wt.% in an interval characterized by a positive $\delta^{13}C$ excursion and elevated metal concentrations (Hammer and Svensen, 2017). The background Cambrian shales at Krekling have still undergone low grade burial metamorphism and the organic matter is overmature, giving very low yields of hydrocarbons during pyrolysis ("dead carbon") (Hammer and Svensen, 2017).

2.2. Sills and aureoles in the Karoo Basin

The dolerite sills in the Karoo Basin (Fig. 1C) are part of the plumbing system that fed the Karoo continental flood basalts (e.g. Chevallier and Woodford, 1999; Svensen et al., 2015), emplaced around 183 Ma (Duncan et al., 1997; Svensen et al., 2012; Gaynor et al., 2022). A large part of these sills intruded the marine to deltaic Ecca Group, metamorphosing organic-rich shales that predominantly make up that sedimentary formation, leading to devolatilization and decarbonatization (Aarnes et al., 2011a; Svensen et al., 2007, 2015).

We investigate three cores from the Ecca Group, which were drilled in 1968 (borehole LA1/68) and 1978 (KL1/78 and DP1/78) (Fig. 1C-F) and contain sills emplaced in the shales. A total of 11 sills are present in the LA1/68 borehole, with a cumulative thickness of 266 m, with the thickest being 199 m (Svensen et al., 2014). Total organic carbon (TOC) data, vitrinite reflectance (Fig. 1F), and aureole models from these boreholes are published in Senger et al., 2015, 2020 and Aarnes et al. (2011a). Here, we show new Hg data from two aureoles around two sills that are both about 15 m thick, and new sulfur data from LA1/68.

In LA1/68, we focus on the contact aureole above the lowermost dolerite sill emplaced at the basement-Ecca contact (Fig. 1F). The sill in KL1/78 is emplaced in the middle of a 15 m-thick organic-rich shale of the Whitehill Formation (Fig. 1D). DP1/78 was drilled 3 km away from KL1/78, and also contains the Whitehill Formation, but without the sill. This makes it possible to compare geochemically similar strata with and without the effects of contact metamorphism.

2.3. Dykes and shale in the Sverdrup Basin, Canada

Sedimentation in the Sverdrup Basin (Fig. 2) was initiated in the Early Carboniferous with rifting of the Ellesmerian orogenic belt (Embry and Beauchamp, 2019). The middle Triassic was marked by active nutrient upwelling and very high bioproductivity leading to deposition of organic rich black shales of the Murray Harbour Formation (Grasby et al., 2016). High Arctic LIP (HALIP) volcanic rocks

were emplaced across the northwestern Arctic Islands (Naber et al., 2020) from the Barremian through to Campanian. Contemporaneous emplacement of sills and dykes occurred across the NE portion of the Sverdrup Basin. A suite of eleven shale samples from the organic-rich Middle Triassic Murray Harbour Formation were collected along a single bedding plane, laterally from the contact with a 1.2 m wide dyke that is located on Raanes Peninsula, Ellesmere Island (78° 31.0′ N 86° 1.8′ W).

3. Methods

3.1. Total organic carbon and sulfur

New TOC measurements from the Oslo Rift locality (Gunhildrød) were done at the Institute for Energy Technology, Kjeller, Norway. We used published TOC and Rock Eval pyrolysis data from the Karoo Basin boreholes (Aarnes et al., 2011a; Svensen et al., 2015) and the Sverdrup Basin (Goodarzi et al., 2018). For TOC, a Leco SC-632 instrument was used following HCl treatment of rock powders to remove carbonate. The samples were introduced into the Leco combustion oven, and the amount of carbon measured as carbon dioxide by an IR-detector. We use 0.2 wt.% TOC as the lower limit for reliable analyses of the organic matter content, as suggested by Grasby et al. (2019), but still show the data below 0.2 wt.% TOC. Rock-Eval 6 instruments were used to identify the type and maturity of organic matter, and to evaluate the hydrocarbon potential of the shales. We use the Hydrogen index (HI) and oxygen index (OI), e.g., Behar et al. (2001), where the mass of released hydrocarbons ("S2") and CO_2 ("S3") during standard pyrolysis in mg is multiplied by 100 and divided by TOC to obtain HI and OI, respectively. S2 values below 0.2 mgHC/gTOC are not considered reliable. The T_{max} parameter, the temperature at which the S2 peak is observed during RockEval analysis, is not considered a reliable proxy for contact metamorphic temperatures (Evenick, 2021) and is not used in this study.

A subset of the samples were analysed for bulk rock elemental sulfur on a FlashSmart CHNS/O a from Thermo scientific at the Department of Geosciences, University of Oslo. Dried and powdered samples were combusted at 1800 °C in a tin sample crucible with a vanadium pentoxide catalyst and the gases analyzed in chromatographic column. For the Sverdrup Basin samples sulfur analyses where conduced by 4-acid digestion of 200 mesh powders analysed by inductively coupled plasma–mass spectrometry.

3.2. Mercury analyses

Mercury analyses were performed at the University of Oxford (UK) using the Lumex RA-915 Portable Mercury Analyzer with a PYRO-915 pyrolyzer attached. Powdered samples (50–100 mg) were weighed and then heated to >700 °C in the pyrolyzer to volatilize the Hg present. The results were calibrated using the NIMT/UOE/FM/001 peat standard with a known Hg concentration of 169 ± 7 ppb, and the NIST-SRM2587 standard for trace elements in soil contaminated with lead from paint (certified Hg concentration of 290 ± 5 ppb). A standard was run after every ten samples in order to assess any effects of sensor drift. Each sample was run in duplicate. Individual analytical errors are ±5%, except where Hg concentrations are <5 ppb, where they are higher due to the greater effect of background noise interfering with peak integration.

3.3. Thermal modelling of sill cooling and contact aureole heating

We used the SILLi 1D numerical model (Iyer et al., 2018), developed to model the thermal effects of sill-related heating of sedimentary rocks and calculate CO_2 generation from heated shales and carbonates. The modelling recreates the thermal effects of sill and dyke emplacement in the Sverdrup Basin and the Karoo Basin. We did not model the temperature evolution of the Oslo Rift contact aureole since it developed around a pluton with a longer and more complex temperature history compared to the other studied sheet intrusions.

The general aspects of the model are described here, with further details given in Iyer et al. (2018). First, each sedimentary layer in the studied basins, including eroded layers, is deposited sequentially in time based on the depositional age. The rate of sedimentation for each layer is then determined by its thickness and the difference in time between its top age and that of the layer deposited before it. A thermal solver computes the temperature within the deposited sedimentary column by applying fixed temperatures at the top and bottom of the strata at every step, calculated from the prescribed geotherm and the energy diffusion equation. This method enables a comparison of the thermal effects of sills with the background burial effects. Sills are emplaced instantaneously at a given time in sedimentary host rocks with a background temperature corresponding to the geothermal gradient at the given depth and time. The model takes into account the heat capacity of melt and the rock types in each case study, and also the latent heat of crystallization in the sills (Aarnes et al., 2010; Iyer et al., 2018).

Dehydration reactions in the host rocks are modelled by modifying the thermal diffusion equation when temperatures of the sediments are increasing within a certain range. We use the EASY%Ro method (Sweeney and Burnham, 1990) to calculate the thermal maturity of the sedimentary rocks. This model uses 20 parallel Arrhenius-type first order reactions to describe the complex process of kerogen breakdown due to temperature increase. Note that the EASY%Ro method leaves 20% of the TOC behind, even close to the sill. Adjustable properties in the thermal model such as melt temperature, geothermal gradient, thermal conductivity, and initial TOC contents were tuned in order to maximize the fit between the modelled and measured vitrinite reflectance and TOC (cf. Iyer et al., 2018). For example, the contact aureole thickness and the maximum aureole temperature can be increased in the model by adjusting the geothermal gradient and the sill temperature. A higher geothermal gradient or sill temperature results in a wider contact aureole at a given depth. The results from the modelling are then compared with aureole proxies from the rocks. Note that the model is set up for instantaneous emplacement of sills and thus does not take into account the possible temperature effects following prolonged emplacement. The uncertainty of the estimated aureole temperature at a given distance will depend on the uncertainty in the input data, and is generally in the ± 25 °C range.

4. Results

4.1. The Oslo Rift

At the Krekling Cambrian shale far from the igneous contact, the succession shows a highly variable TOC content. The shales reach 14 wt.% TOC at maximum, with abundant pyrite nodules (Hammer and Svensen, 2017) even though the section is low grade metamorphic. The sulfur content in these shales is mostly below 1 wt.%, with an exception of 3.6 wt.%. Hg contents show a positive correlation with TOC despite the thermal maturity of the organic matter (see above) and reach a maximum concentration of 503 ppb (Fig. 3 and Table S1). There is no apparent correlation with sulfur. The average Hg content in the most organic-rich interval is 282 ppb. The shale is thermally mature, as shown by RockEval and the very low potential for the organic matter to generate hydrocarbons and CO_2 (Table S1).

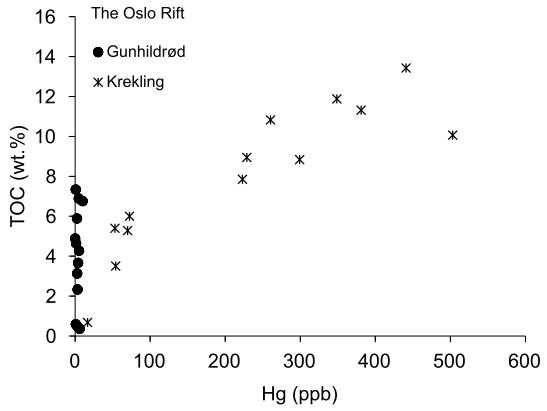

Fig. 3. Relationship between the TOC and Hg content in Cambrian shale from Krekling and the hornfels from Gunhildrød.

At Gunhhildrød, a few km away, the same succession experienced high temperature contact metamorphism around a granitic pluton. Based on the mineralogy of the contact aureole, the minimum peak temperature was around 500 °C (Svensen and Jamtveit, 1998). Our data from the contact aureole at Gunhildrød show that the TOC is lowered in the aureole (0.5–7.3 wt.%) compared to the reference section at Krekling (maximum values of 13.5 wt.%). During metamorphism, the organic matter was transformed to graphite and the TOC measurements represent the graphite content. The Hg content in the shale from the contact aureole is as low as 0–6 ppb with an average of 3.4 ppb, i.e. below the limit of measurement reliability, whereas the sulfur content is higher compared to samples from the reference section (average of 1.8 and 0.9 wt.% S, respectively).

4.2. LA1/68 in the Karoo Basin

The measured TOC in the contact aureole varies from zero in the innermost 5 m of the aureole to maximum values of >2 wt.% in the background strata (Fig. 4 and Table S2). Vitrinite reflectance ranges from 1.0%Ro outside the contact aureole, to the highest values of 5.7%Ro at 9.2 m above the sill. This corresponds to a normalized distance of 0.8 (i.e., the distance from the sill contact divided by the sill thickness). Closer to the sill, the vitrinite values decrease notably and the quality of the vitrinite is reduced, with the exception of the 4.1%Ro value at the contact. Such a breakdown of vitrinite is a common feature in the high temperature part of contact aureoles where the vitrinite is exposed to supercritical fluids. Note that TOC content is below the 0.2 wt.% reliability limit in the innermost 5.2 m of the aureole (0.3 normalized distance). The potential to generate hydrocarbon, shown by the S2 values (Fig. 4), decreases towards the sill contact, but the increasing OI suggest oxidation of the organic matter, consistent with the vitrinite data.

The Hg content follows TOC and has values around 40–50 ppb outside the aureole, and 10–25 ppb in the outer aureole. In the innermost 5 m of the aureole (0.3 normalized distance), Hg is reduced to 4–38 ppb (Table S2). 38 ppb Hg is measured in the sample analysed from the direct contact with the sill where the TOC is very low (0.03 wt.%), but sulfides are abundant (Fig. 1E) even though their specific zone was not included in the analyzed sample. For this reason, the Hg/TOC deviates from the values obtained elsewhere in the aureole as some Hg is likely incorporated into the sulfides. The bulk sulfur content in the aureole is zero in the innermost zone where the organic matter is oxidized, and is low (0.4–0.6 wt.%) in the rest of the analyzed section, with no correlation to the inward decrease in Hg content. The increase in Hg/TOC in the innermost 5 metres of the aureole is likely due to the very low TOC content. The maximum temperature modelled

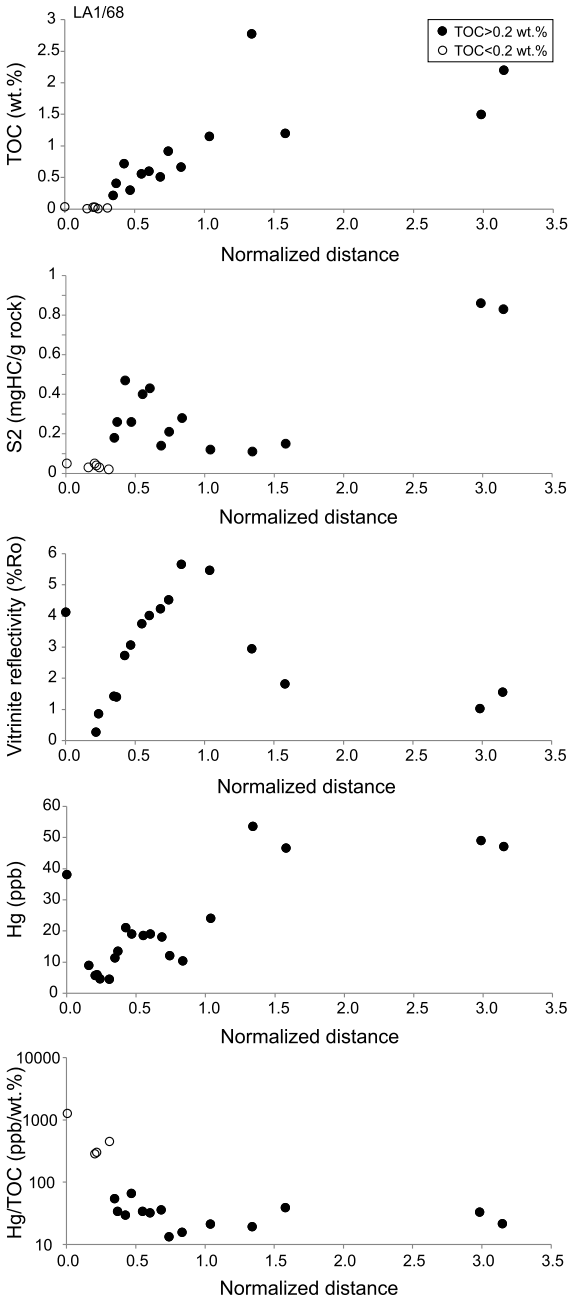

Fig. 4. Geochemical data from the contact aureole above the 15 m thick sill in the basal part of LA1/68. The sample distance from the intrusion contact is normalized to the sill thickness. The somewhat elevated Hg (38 ppb) at the contact with the sill is likely due to the presence of a centimetre-thick zone with sulfides.

at the sill contact is 750 °C whereas the background temperature outside the aureole is 215 °C.

4.3. KL1/78 and DP1/78 in the Karoo Basin

The unmetamorphosed sedimentary rocks of the Ecca Group in DP1/78 show variable TOC contents, from 0.48 to 14.4 wt.% (Table S2). The highest values are from the Whitehill Formation shale. The organic matter shows a relatively low thermal maturity (average vitrinite reflectivity of 0.7%) and a high hydrocarbon production potential (S2 between 3.8 and 22 mg/g) (Aarnes et al., 2011a; Fig. 5). The average Hg content of the Whitehill Formation samples is 214 ppb, spanning from a low of 22 ppb and a high of 476 ppb. The range in sedimentary Hg concentrations across the

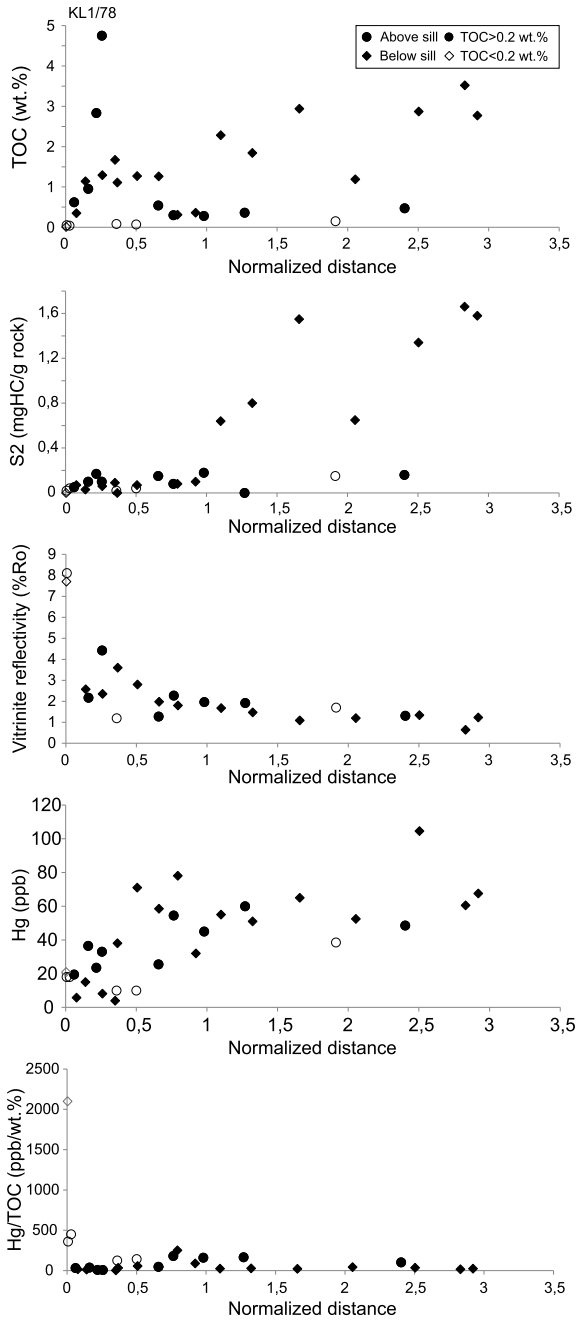

Fig. 5. Geochemical data from the contact aureole above and below the 15 m thick sill in KL1/78. The sample distance from the intrusion contact is normalized to the sill thickness.

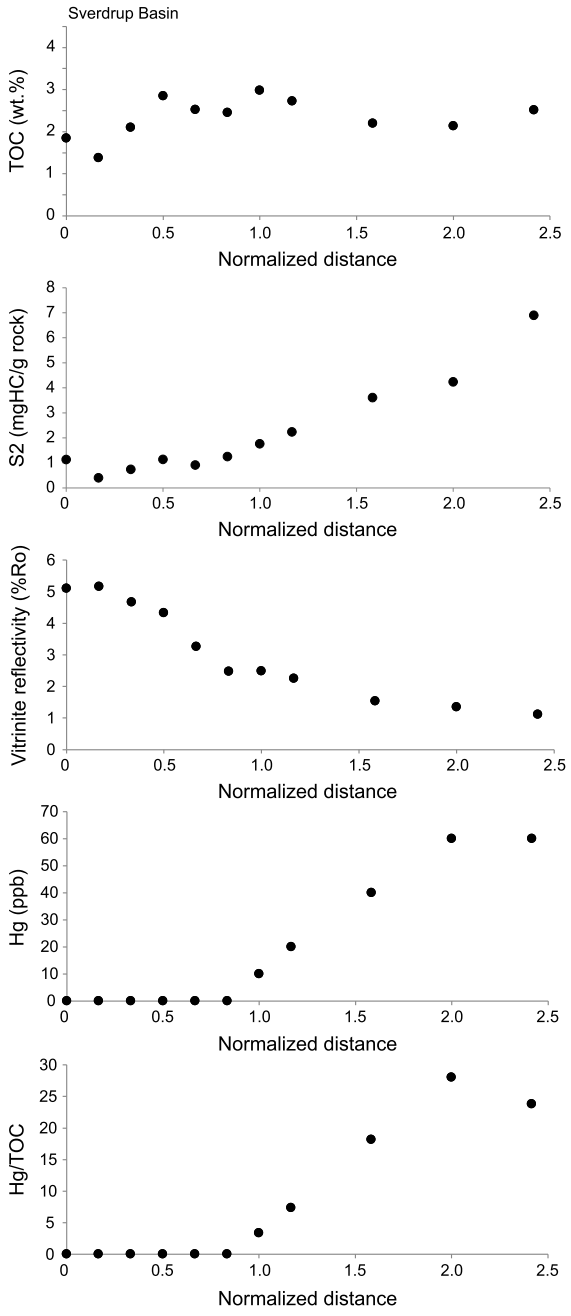

Fig. 6. Geochemical data from the contact aureole around the 1.2 m wide dyke from the Sverdrup Basin. The sample distance from the intrusion contact is normalized to the dyke width.

formation stratigraphy are likely not only due to variations in the TOC content as the Hg/TOC ratio varies between 1 and 109 (average of 62; Table S2).

The contact aureole developed in the Whitehill Formation (borehole KL1/78, Fig. 5) features a gradual reduction in TOC content towards the sill contact, where it approaches zero (<0.04 wt.%) and the RockEval hydrocarbon and CO_2 generation potential is also reduced to zero in the aureole. In the innermost 1 m of the aureole (normalized distance of 0.1 in Fig. 5), the TOC is lower than 0.6 wt.% in all samples and the Hg is between 6 and 18 ppb. Since the sill is emplaced in the middle of the Whitehill Formation, we lack a full aureole profile developed within that unit and the aureole extends into the shale-dominated Prince Albert and Tierberg formations (Figs. 2B and 7). Vitrinite data demonstrate high temperature metamorphism near the sill, with values up to 8%Ro (Fig. 5).

4.4. The Sverdrup Basin

In the contact aureole around the 1.2 m wide dyke in the Sverdrup Basin (Fig. 6), TOC contents drop to 1.4 wt.%, compared to background levels of 2.1–4.0 wt.% (Table S3). This effect is only recorded in the innermost three samples (<0.5 m) of the aureole. The S2 of the aureole shows a linear decrease towards the contact ($R^2 = 0.89$) whereas the OI shows a minor decrease in the outer aureole and higher values in the innermost 20 cm indicating oxidation of the organic matter. The Hg shows a great decrease due to the metamorphism and is reduced from background values of 60 ppb to below measurable levels 1 m from the contact (normal-

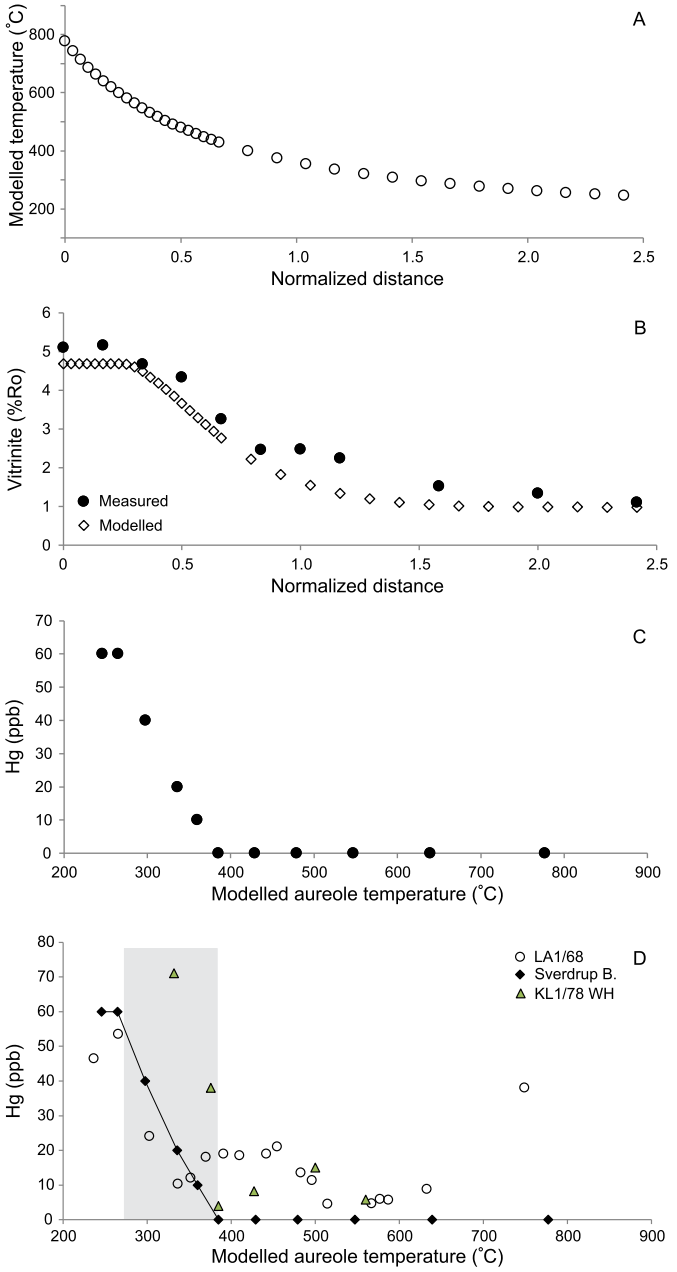

Fig. 7. Data and model results from the Sverdrup Basin dyke. **A**) Modelled aureole temperature. **B**) Modelled and measured vitrinite reflectance. **C**) Mercury content in the aureole plotted against modelled temperature of the aureole. **D**) Mercury content in the three modelled aureoles. The grey box shows the main temperature interval where the Hg rapidly declines from background values. The line is drawn between the data points from the dyke in the Sverdrup Basin.

ized distance of 0.8, Fig. 6). The sulfur content in the shale is low in the outer aureole (up to 0.9 wt.% S), and decreases to below 0.1 wt.% at 1.2 m from the contact (Table S3). The data set with values above the detection limit is too small (4 samples) to fully evaluate the potential covariance between Hg, S, and TOC. Interestingly, the width of the contact aureole depends on the proxy used. In our case, both the Hg and vitrinite aureoles start at around 1.8 normalized distance from the contact, and the TOC aureole from 0.3 normalized distance (0.4 m) from the contact with the dyke. By combining the geochemical data with modelling of conductive heat transport, a 33% decrease in Hg in the temperature interval 265–300 °C is calculated (Fig. 7). Additionally, Hg contents fall gradually towards the contact, even while the TOC remains steady at background values and the shale only experienced intermediate metamorphic temperatures. At >385 °C (<1 m from the contact) the Hg content in the shale is negligible.

5. Discussion

5.1. Representative cases and aureole proxies

The contact aureoles presented in this study represent realistic and illustrative cases for investigating the behaviour of Hg during contact metamorphism associated with LIPs. We cover examples of aureoles related to a pluton, sills, and a dyke, from outcrops and from boreholes. However, even though contact metamorphism is a well understood process (cf. Kerrick, 1991), comparing data from different contact aureoles is challenging. These difficulties are due to both the variability between geological settings (e.g., sill/dyke thickness and temperature, depth of emplacement, geothermal gradients, weathering and preservation), and which aureole proxies are used (Aarnes et al., 2012). Some data, such as TOC, pyrolysis data, and $\delta^{13}C$ compositions of the organic matter, are very useful when sampling geochemically homogeneous layers across the aureole. However, when studying aureoles around sills, sampling is generally perpendicular to stratigraphy; thus, the TOC aureole profiles represent the thermal effects in addition to any original stratigraphic variations. This complexity makes the contact metamorphic effects harder to isolate and interpret, cf. the data scatter from the KL1/78 aureole from the Karoo Basin (Fig. 5), often resulting in a poor model-data fit. Contact aureoles around dykes may be easier to interpret as aureole samples can be collected from a specific sedimentary horizon with increasing horizontal or at least sub-vertical distance from the dyke contact. Investigating single stratigraphic horizons makes it easier to understand and quantify how the aureole geochemistry and proxies are affected by the heating. However, dykes in sedimentary basins are usually thin compared to sills, which means that they may not result in high temperature aureoles with hornfels and a full or significant transformation of TOC to CH_4 or CO_2. And they are less likely to be good analogues for the large magmatic intrusions associated with LIP formation.

The evolution and extent of a contact aureole and its mineralogy depends on the thickness or volume of the intrusions, in addition to the emplacement temperature of the magma and the thermal properties of the sedimentary rocks. For example, a thick sill (50–100 m) results in a well-developed aureole, whereas thin sills (less than a few m) may be associated with no apparent visual metamorphic effects. Still when analyzed, thin sheet intrusions usually have aureoles sharing some of the key proxy characteristics as thick sheets, e.g., a reduction in TOC content towards the contact, and a decrease in the potential to generate hydrocarbons and CO_2 as shown by pyrolysis parameters such as S2 and HI (e.g., Agirrezabala et al., 2014). As these factors usually vary between case studies, the aureoles have to be compared and interpreted with care.

The 1.2 m wide dyke from the Sverdrup Basin shows a similar aureole trend to the 15 m thick sills from the Karoo Basin, with a gradual TOC reduction towards the contact and an increase in vitrinite reflectance. The innermost zone around thick sills, where hornfels is developed, is characterized by a complete loss of the initial organic matter, or the presence of graphite if the initial sedimentary TOC was high (as is typical for a organic-rich shale). The sulfur (bound to pyrite or organic matter) is also affected by contact metamorphism and is often but not always (e.g., the Oslo Rift case) lowered towards intrusion contacts (Yallup et al., 2013). The Sverdrup Basin case stands out as our most illustrative case for understanding the behaviour of Hg during aureole heating, as it was possible to sample perpendicular to the dyke contact along a single bedding plane in adjacent shale.

5.2. Behaviour of Hg in a contact aureole

During heating in a contact aureole, both the hydrous minerals and the organic matter are gradually devolatilized (cf. Aarnes et al., 2010). The organic matter releases carbon-bearing compounds, eventually lowering both the bulk rock TOC content and reducing the potential for the remaining organic matter to generate hydrocarbons (e.g., lowered S2, S3, HI and OI values). This process of devolatilization is independent of the type of organic matter present in the contact aureoles (e.g., Agirrezabala et al., 2014) as also shown in our case studies, resulting in low-TOC and low S2 and HI aureoles. During heating, the organic matter is structurally transformed towards higher crystallinity, and above ca. 650 °C the transition to graphite is considered complete (e.g., Beyssac et al., 2003). Graphite formation depends on the timescale of metamorphism, with long timescales, such as those expected for contact aureoles around plutons, making this process more likely to occur (Beyssac et al., 2003; Mori et al., 2017).

In the Oslo Rift case, TOC is present as graphite in the aureole, whilst the Hg concentrations are very low and close to the limit of detection (Table S1). The relationship between TOC and Hg in several of our cases (Fig. 3 and Table S2) shows that organic matter is the main host of the Hg, demonstrated from the Oslo Rift case by a R^2 value of 0.79. The co-variation is also evident from LA1/68 ($R^2 = 0.76$, excluding data from the innermost 4.6 m of the aureole where the TOC is below 0.2 wt.%) whereas the KL1/78 and Sverdrup Basin cases show a large scatter due to limited TOC loss in the outer aureole (Sverdrup Basin) and stratigraphic variations in the initial TOC (KL1/78). Note the samples from the Sverdrup Basin and the Oslo Rift were collected from outcrops. Weathering may result in preferential loss of Hg relative to TOC in shale, and moreover a lowering of the shale HI and an increase in the OI (e.g., Charbonnier et al., 2020; Park et al., 2022). We carefully avoided weathered zones during sampling and our aureole data from outcrops show consistent trends as a function of the distance to the intrusions, suggesting a minimal weathering effect on TOC and Hg at our study sites. This conclusion is, moreover, supported by the fact that the samples with the lowest Hg, HI, and OI values come from the contact aureole, and that metamorphism makes the rocks more resistant to weathering than background shale.

Significant Hg may be bound to pyrite in certain depositional environments (Shen et al., 2019, 2020) adding complexity when interpreting co-variation between elements in contact aureoles. In our dataset we do not find any correlation between S and TOC, or S and Hg/TOC (Fig. 8), supporting a dominant organic host of the mercury. Thus it is expected that loss of TOC during metamorphism would be accompanied by a lowering of Hg contents (Fig. 7D). The only potential exception to organic-affiliated Hg in our data is the somewhat elevated Hg in the innermost sample from the LA1/68 contact aureole (38 ppb versus 5–9 ppb in other samples; Table S2). In the 38 ppb sample, the hornfels contains a ~0.5 cm-thick zone with sulfides at the sill-sediment contact, representing a local phenomena on this sub-cm scale.

In short-lived contact aureoles, such as around the thin dyke in the Sverdrup Basin, less than half (35%) of the TOC from within the innermost 20 cm of the contact aureole (average TOC of 1.6 wt.%) is lost compared to the background rock content (average TOC of 2.5 wt.%). Still, the Hg is completely lost from the contact aureole, showing the strong effect of aureole temperature on Hg devolatilization (Fig. 7D). The aureole model from the Sverdrup Basin case shows that the content of Hg is reduced from background levels starting from a temperature of about 270 °C (Fig. 7D). The Hg is further reduced to zero at 385 °C, whereas the TOC remains unaffected until 60 cm from the contact (corresponding to 480 °C). The lowering of Hg from around 1.9 m from the contact corresponds to where the organic matter shows a geochemical response

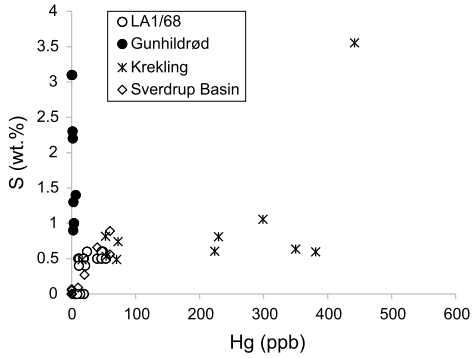

Fig. 8. Comparison between bulk rock total sulfur and Hg content. Pyrite-bound Hg should have resulted in positive trends between S and Hg.

to the heating. At that distance, the pyrolysis S2 parameter (Fig. 6), shows a decline from background values, indicating that the kerogen in the aureole was affected by thermal devolatilization. This is also the distance from the contact at which the vitrinite reflectance starts to increase from background values.

Our cases show that the organic-rich shales lost a significant fraction of the Hg during the contact metamorphism and that the Hg migrated out of the aureoles. Moreover, permeable pathways and fractures are common along sill/dyke contacts, and degassing pipes generated from phreatic eruptions and hydrothermal vent complexes are frequent phenomena in these settings (Svensen et al., 2007, 2020; Aarnes et al., 2012; Senger et al., 2015; Galerne and Hasenclever, 2019). Mercury-rich deposits are not known in either of the study areas, making it likely that the Hg migrated out of the contact aureoles and perhaps fully out of the basins.

5.3. Implications for LIP-related studies

The remaining Hg content in the innermost contact aureoles is negligible. Therefore, Hg devolatilization from sediments following contact metamorphism appears to be highly efficient, liberating the majority of Hg from sedimentary rocks within the high temperature parts of contact aureoles. In our case studies, this translates to 60–250 ppb Hg liberation. From a bulk contact aureole perspective, the net Hg loss can be estimated from the aureole thickness and the areal extent of the sill-aureole system. Thus an upscaling of the Hg loss from individual aureoles to a LIP scale is possible, but critically depends on how well characterized the sill/dyke-basin system is.

Many (though not all) continental LIPs are characterized by intrusion through sedimentary basins with abundant sills and dykes (e.g., Chevallier and Woodford, 1999; Svensen et al., 2014). Our measurements here and those of Aarnes et al. (2012) indicate that the volume of a contact aureole is related to the sill volume, with an aureole volume roughly double the sill volume (a 1:1 thickness relationship on both sides of a sill). We can use this relationship as a way to estimate the aureole volume on a basin scale. Similar approaches have been used to quantify the generation of thermogenic carbon emissions from LIPs (cf. Svensen et al., 2004). The actual volumes used for individual sills or pulses of sills, require detailed field and/or seismic mapping and a consideration of the original volume. Due to these case-dependent complexities, we use our data only from the Karoo Basin, which is the best geologically characterized basin included in our study, as a case to further understand the importance of thermogenic Hg sources. Previous work has shown that a significant volume of sills were emplaced into the Ecca Group shale of the Karoo Basin in a short time period (ca. 100k years) between 183.147 ± 0.059 Ma and 183.187 ± 0.133 Ma, broadly coeval with the Toarcian Oceanic Anoxic Event (Gaynor et

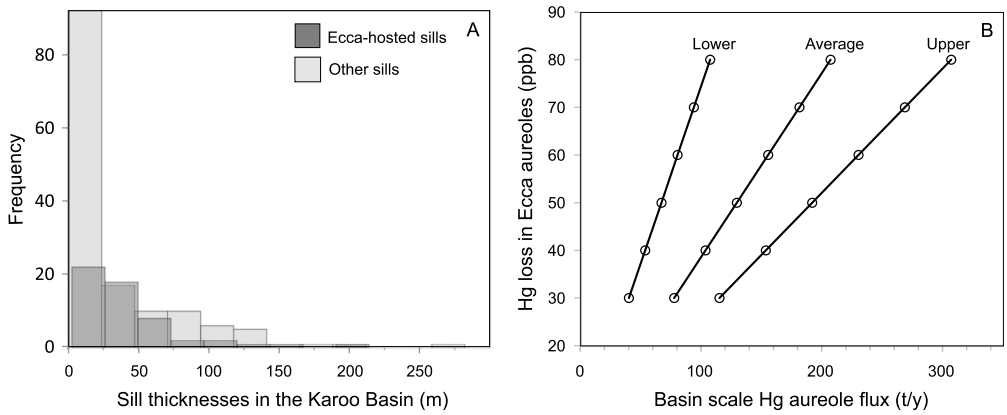

Fig. 9. A) Histogram of sill thicknesses from the Karoo Basin grouped according to whether they are emplaced in the Ecca Groups shale or in other formations. Data from Svensen et al. (2014). **B**) Results from upscaling the loss of Hg in contact aureoles to basin scale fluxes averaged over 100 kyr of sill emplacement. The three lines are derived from the average (108,000 km^3), lower (56,000 km^3) and upper (160,000 km^3) estimates of the proportion of Ecca Group aureole volumes where Hg is significantly affected. These volumes are derived from using 1/3 of the Karoo Basin sill volume (270,000±130,000 km^3) multiplied with a factor 1.2 to account for the relevant aureole volume with Hg loss.

al., 2022). The number of sills vary from 0 to 10 in boreholes penetrating the Ecca group within the basin, locally comprising 55% of the Ecca Group stratigraphy and up to a total of 315 m of sills (Svensen et al., 2014). The volume of the sills emplaced in the Karoo Basin is estimated as $270,000 \pm 130,000$ km^3 with 1/3 of the total volume representing sills emplaced in the Ecca Group shales (Svensen et al., 2014; Fig. 9A). The Karoo cases presented here show a significant Hg loss from normalized distances of about 0.6 of aureole width. This implies that multiplying the sill volume by 1.2 will estimate the high temperature part of the aureole with Hg loss (0.6 times the aureole volume on each side of the sills, see above). Note that this approach will provide an upper limit to the Hg loss in cases where the sills are closely spaced and the contact aureoles overlap (cf. Aarnes et al., 2011a).

The results from the Ecca Group aureoles account for Hg losses between 30 and 80 ppb (Fig. 4, 5), giving a range in Hg mobilized from the aureole reservoir of 72–192 t per km^3 of aureole (assuming a shale density of 2.4 g/cm^3). This yields a total emission of 4–31 Mt Hg from aureoles of the Ecca Group (taking the aureole volumes where Hg is significantly reduced as 56,000–160,000 km^3 of affected country rock). The Hg flux from the contact aureoles will depend on the details of sill emplacement and the likely pulsed nature of the emplacement, but when assuming 100 kyr years of basin scale sill emplacement in the Ecca Group (Gaynor et al., 2022), thermogenic release plausibly averaged Hg fluxes of 78–207 t/year (Fig. 9B). In a scenario with pulsed emplacement spanning a time interval of 10 kyr years, the flux will be considerably higher.

Although there are many uncertainties with these basin-scale, thermogenic estimates of Hg fluxes, they are based on direct measurements of the Hg source rocks and fully independent of estimates of other LIP magmatic volatile fluxes. Estimates of the magmatic Hg flux from the Karoo LIP by scaling with proposed SO_2 emissions suggest that the entire emplacement may have emitted up to 150 Mt of Hg over an emplacement period of ~1 Myr (Percival et al., 2015), but again with possible pulses of heightened activity. Of significance is that the estimated igneous Hg release per unit lava is 75 t/km^3 lava (Percival et al., 2015), and that the average thermogenic Hg release estimate is up to three times higher (72–192 t/km^3). For further comparison, the estimates for the current annual global volcanic Hg emissions vary considerably, with values from 46–106 t/y (Pyle and Mather, 2003; Edwards et al., 2021).

Although magmatic degassing of Hg is not well understood, our new data suggest that during periods of LIP activity in the Karoo when intrusive activity was equal to or greater than extrusive, thermogenic Hg fluxes might plausibly have dominated the magmatic source. We conclude that LIP sills emplaced in organic-rich rocks may have affected the global Hg cycle during parts of their formation history. Furthermore this process was likely particularly relevant for LIPs with a significant sill and organic-rich sedimentary association such as the Karoo LIP, the Central Atlantic Magmatic Province, the Siberian Traps, and the North East Atlantic Igneous Province (e.g., Heimdal et al., 2020; Svensen et al., 2004, 2009; Black et al., 2021). These nuances highlight the complexity associated with interpreting perturbations of the global Hg cycle during times of LIP formation, and the interactions between these vast episodes of volcanism and the wider Earth system.

6. Conclusions

Understanding mercury release during contact metamorphism when volcanics intrude into sediments is important in terms of understanding the Hg signals associated with LIPs recorded in the geological record. We have studied four representative contact aureoles developed in shale around a granitic pluton (the Oslo Rift), two dolerite sills (the Karoo Basin), and a dyke (the Sverdrup Basin). We combined measurements of key aureole parameters with new mercury measurements and thermal modelling in order to understand the changes in Hg concentrations with increasing thermal maturity. We show that the shale-hosted Hg is bound to the organic matter, and that the sedimentary content of both Hg and TOC in the shale decrease with increasing maturity and metamorphic grade towards the contact with the igneous intrusions. The Hg content is reduced to negligible values during contact metamorphism, demonstrating the efficiency of Hg loss from the sediments and the aureoles. Thermal modelling of the aureoles surrounding the sills and the dyke enable a quantification of the temperature interval where this loss takes place. We show that Hg mobilization from the aureoles begins at temperatures around 265–300 °C. We estimate that the thermogenic Hg release per km^3 of aureole may be up to three times higher than from the equivalent volume of erupted/intruded igneous rocks. Thermogenic Hg total emissions from the Ecca Group shales in the Karoo Basin are estimated 4-31 Mt Hg with fluxes maybe as high as 78–207 t/y (maximum 307 t/y) when averaged over 100,000 years of sill emplacement. The pulsed nature of intrusive volcanism suggests that this flux may be considerably higher and could dominate LIP emissions during some periods of their life span. Our findings have major implications for the understanding of the solid Earth part

of the Hg cycle. Mercury anomalies in sedimentary rocks can be explained by rapid devolatilization and Hg loss following LIP-scale sill emplacement in organic-rich lithologies.

CRediT authorship contribution statement

Henrik H. Svensen: Writing – review & editing, Writing – original draft, Validation, Project administration, Methodology, Investigation, Funding acquisition, Formal analysis, Data curation, Conceptualization. **Morgan T. Jones:** Writing – review & editing, Writing – original draft, Methodology, Investigation, Conceptualization. **Lawrence M.E. Percival:** Writing – review & editing, Writing – original draft, Validation, Investigation, Conceptualization. **Stephen E. Grasby:** Writing – review & editing, Writing – original draft, Investigation, Data curation, Conceptualization. **Tamsin A. Mather:** Writing – review & editing, Writing – original draft, Validation, Methodology, Funding acquisition, Formal analysis, Conceptualization.

Declaration of competing interest

The authors declare that they have no known competing financial interests or personal relationships that could have appeared to influence the work reported in this paper.

Data availability

Data will be made available on request.

Acknowledgements

We gratefully acknowledge support from the Norwegian Research Council (grant number 263000 to M.T.J., and grant number 223272 to CEED). We also would like to thank the Council of Geoscience and the National Core Library in South Africa, for access to cores. T.A.M. acknowledges funding from ERC consolidator grant (ERC-2018-COG-818717-V-ECHO). LMEP thanks the Research Foundation – Flanders (FWO: grant 12P4522N) for funding. We would also like to thank Sverre Planke and Øyvind Hammer for discussions, fieldwork, and lasting enthusiasm, and Michael Heeremans for providing the map in Fig. 1A.

Appendix A. Supplementary material

Supplementary material related to this article can be found online at https://doi.org/10.1016/j.epsl.2023.118306.

References

Aarnes, I., Fristad, K., Planke, S., Svensen, H., 2011b. The impact of host-rock composition on devolatilization of sedimentary rocks during contact metamorphism around mafic sheet intrusions. G-Cubed v12, G10019. https://doi.org/10.1029/2011GC003636.

Aarnes, I., Podladchikov, Y., Svensen, H., 2012. Devolatilization-induced pressure build-up: implications for reaction front movement and breccia pipe formation. Geofluids 12 (4), 265–279.

Aarnes, I., Svensen, H., Connolly, J.A.D., Podladchikov, Y.Y., 2010. How contact metamorphism can trigger global climate changes: modeling gas generation around igneous sills in sedimentary basins. Geochim. Cosmochim. Acta 74 (24), 7179–7195.

Aarnes, I., Svensen, H., Polteau, S., Planke, S., 2011a. Contact metamorphic devolatilization of shales in the Karoo Basin, South Africa, and the effects of multiple sill intrusions. Chem. Geol. 281 (3–4), 181–194.

Agirrezabala, L.M., Permanyer, A., Suárez-Ruiz, I., Dorronsoro, C., 2014. Contact metamorphism of organic-rich mudstones and carbon release around a magmatic sill in the Basque-Cantabrian Basin, western Pyrenees. Org. Geochem. 69, 26–35.

Bagnato, E., Aiuppa, A., Parello, F., Calabrese, S., D'Alessandro, W., Mather, T.A., McGonigle, A.J.S., Pyle, D.M., Wängberg, I., 2007. Degassing of gaseous (elemental and reactive) and particulate mercury from Mount Etna volcano (Southern Italy). Atmos. Environ. 41, 7377–7388. https://doi.org/10.1016/j.atmosenv.2007.05.060.

Behar, F., Beaumont, V., De B. Penteado, H.L., 2001. Rock-eval 6 technology: performances and developments. Oil Gas Sci. Tech. - Rev. IFP 56 (2), 111–134. https://doi.org/10.2516/ogst:2001013.

Beyssac, O., Brunet, F., Petitet, J.P., Goffé, B., Rouzaud, J.N., 2003. Experimental study of the microtextural and structural transformations of carbonaceous materials under pressure and temperature. Eur. J. Mineral. 15, 937–951.

Black, B.A., Lamarque, J.F., Shields, C.A., Elkins-Tanton, L.T., Kiehl, J.T., 2014. Acid rain and ozone depletion from pulsed Siberian Traps magmatism. Geology 42 (1), 67–70.

Black, B.A., Karlstrom, L., Mather, T.A., 2021. The life cycle of large igneous provinces. Nat Rev Earth Environ 2, 840–857. https://doi.org/10.1038/s43017-021-00221-4.

Bond, D.P.G., Grasby, S.E., 2017. On the causes of mass extinctions. Palaeogeogr. Palaeoclimatol. Palaeoecol. 478, 3–29.

Caldeira, K., Rampino, M.R., 1990. Carbon dioxide emissions from Deccan volcanism and a K/T boundary greenhouse effect. Geophys. Res. Lett. 17.

Charbonnier, G., Adatte, T., Föllmi, K.B., Suan, G., 2020. Effect of intense weathering and postdepositional degradation of organic matter on Hg/TOC proxy in organic-rich sediments and its implications for deep-time investigations. Geochem. Geophys. Geosyst. 21, e2019GC008707. https://doi-org.ezproxy.uio.no/10.1029/2019GC008707.

Chevallier, L., Woodford, A., 1999. Morpho-tectonics and mechanism of emplacement of the dolerite rings and sills of the western Karoo, South Africa. S. Afr. J. Geol. 102 (1), 43–54.

Courtillot, V.E., Renne, P.R., 2003. On the ages of flood basalt events. C. R. Geosci. 335 (1), 113–140. https://doi.org/10.1016/S1631-0713(03)00006-3.

Duncan, R.A., Hooper, P.R., Rehacek, J., Marsh, J., Duncan, A.R., 1997. The timing and duration of the Karoo igneous event, southern Gondwana. J. Geophys. Res., Solid Earth 102, 18127–18138.

Edwards, B.A., Kushner, D.S., Outridge, P.M., Wang, F., 2021. Fifty years of volcanic mercury emission research: knowledge gaps and future directions. Sci. Total Environ. 757, 143800. https://doi.org/10.1016/j.scitotenv.2020.143800.

Embry, A.F., Beauchamp, B., 2019. Sverdrup Basin. In: Miall, Edited by A. (Ed.), The sedimentary basins of the United States and Canada, 2nd, pp. 559–592.

Evenick, J.C., 2021. Examining the relationship between Tmax and vitrinite reflectance: an empirical comparison between thermal maturity indicators. J. Nat. Gas Sci. Eng. 91, 103946. https://doi.org/10.1016/j.jngse.2021.103946.

Frieling, J., Mather, T.A., März, C., Jenkyns, H.C., Hennekam, R., Reichart, G.-J., Slomp, C.P., van Helmond, N.A.G.M., 2023. Effects of redox variability and early diagenesis on marine sedimentary Hg records. Geochim. Cosmochim. Acta 351, 78–95. https://doi.org/10.1016/j.gca.2023.04.015.

Galerne, C.Y., Hasenclever, J., 2019. Distinct degassing pulses during magma invasion in the stratified Karoo Basin—New insights from hydrothermal fluid flow modeling. Geochem. Geophys. Geosyst. 20, 2955–2984.

Ganino, C., Arndt, N.T., 2009. Climate changes caused by degassing of sediments during the emplacement of large igneous provinces. Geology 37 (4), 323–326.

Gaynor, S.P., Svensen, H.H., Polteau, S., Schaltegger, U., 2022. Local melt contamination and global climate impact: dating the emplacement of Karoo LIP sills into organic-rich shale. Earth Planet. Sci. Lett. 579. https://doi.org/10.1016/j.epsl.2022.117371.

Goodarzi, F., Gentzis, T., Grasby, S.E., Dewing, K., 2018. Influence of igneous intrusions on thermal maturity and optical texture: comparison between a bituminous marl and a coal seam of the same maturity. Int. J. Coal Geol. 198, 183–197. https://doi.org/10.1016/j.coal.2018.09.013.

Grasby, S.E., Sanei, H., Beauchamp, B., 2011. Catastrophic dispersion of coal fly ash into oceans during the latest Permian extinction. Nat. Geosci. 4, 104–107.

Grasby, S.E., Beauchamp, B., Knies, J., 2016. Early Triassic productivity crises delayed recovery from world's worst mass extinction. Geology 44 (9), 779–782.

Grasby, S.E., Shen, W., Yin, R., Gleason, J.D., Blum, J.D., Lepak, R.F., Hurley, J.P., Beauchamp, B., 2017. Isotopic signatures of mercury contamination in latest Permian oceans. Geology 45, 55–58.

Grasby, S.E., Them II, T.R., Chen, Z., Yin, R., Ardakani, O.H., 2019. Mercury as a proxy for volcanic emissions in the geologic record. Earth-Sci. Rev. 196, 102880.

Guo, S., Zhang, L., Niu, X., Gao, L., Cao, Y., Wei, X-X., Li, X., 2018. Mercury release characteristics during pyrolysis of eight bituminous coals. Fuel 222, 250–257. https://doi.org/10.1016/j.fuel.2018.02.134.

Hammer, Ø, Svensen, H.H., 2017. Biostratigraphy and carbon and nitrogen geochemistry of the SPICE event in Cambrian low-grade metamorphic black shale, Southern Norway. Palaeogeogr. Palaeoclimatol. Palaeoecol. 468, 216–227.

Heeremans, M., Faleide, J.I., Larsen, B.T., 2004. Late Carboniferous - Early Permian of NW Europe: an introduction to a new regional map. Geol. Soc. Spec. Publ. (ISSN 0305-8719) 223 (8719), 75–88.

Heimdal, T.H., Goddéris, Y., Jones, M.T., Svensen, H.H., 2021. Assessing the importance of thermogenic degassing from the Karoo Large Igneous Province (LIP) in driving Toarcian carbon cycle perturbations. Nat. Commun. 12, 6221. https://doi.org/10.1038/s41467-021-26467-6.

Heimdal, T.H., Jones, M.T., Svensen, H.H., 2020. Thermogenic carbon release from the Central Atlantic Magmatic Province caused major end-Triassic carbon cycle perturbations. Proc. Natl. Acad. Sci. https://doi.org/10.1073/pnas.2000095117.

Iyer, K., Svensen, H.H., Schmid, D.W., 2018. SILLi 1.0: a 1D numerical tool quantifying the thermal effects of sill intrusions. Geoscientific model development. https://doi.org/10.5194/gmd-2017-132.

Jamtveit, B., Bucher-Nurminen, K., Stijfhoorn, D.E., 1992. Contact metamorphism of layered shale-carbonate sequences in the Oslo Rift: I. Buffering, infiltration, and the mechanisms of mass transport. J. Petrol. 33 (2), 377–422.
Jones, M.T., Jerram, D.A., Svensen, H.H., Grove, C., 2016. The effects of large igneous provinces on the global carbon and sulphur cycles. Palaeogeogr. Palaeoclimatol. Palaeoecol. 441, 4–21.
Jones, M.T., Percival, L.M.E., Stokke, E.W., Frieling, J., Mather, T.A., Riber, L., Schubert, B.A., Schultz, B., Tegner, C., Planke, S., Svensen, H.H., 2019. Mercury anomalies across the Palaeocene–Eocene Thermal Maximum. Clim. Past 15 (1), 217–236.
Kerrick, D.M., 1991. Overview of contact metamorphism. In: Kerrick, D.M. (Ed.), Contact Metamorphism, Reviews in Mineralogy, vol. 26, pp. 1–12.
Larson, R.L., Erba, E., 1999. Onset of the Mid-Cretaceous greenhouse in the Barremian-Aptian: igneous events and the biological, sedimentary, and geochemical responses. Paleoceanography 14 (6), 663–678. https://doi.org/10.1029/1999PA900040.
Liu, Z., et al., 2022. Mercury loss and isotope fractionation during thermal maturation of organic-rich mudrocks. Chem. Geol. 612, 121144.
McElwain, J.C., Wade-Murphy, J., Hesselbo, S.P., 2005. Changes in carbon dioxide during an oceanic anoxic event linked to intrusion into Gondwana coals. Nature 435 (7041), 479–482.
Mori, H., Mori, N., Wallis, S., Westaway, R., Annen, C., 2017. The importance of heating duration for Raman CM thermometry: evidence from contact metamorphism around the Great Whin Sill intrusion, UK. J. Metamorph. Geol. 35, 165–180. https://doi-org.ezproxy.uio.no/10.1111/jmg.12225.
Naber, T.V., Grasby, S.E., Cuthbertson, J.P., Rayner, N., Tegner, C., 2020. New constraints on the age, geochemistry, and environmental impact of High Arctic Large Igneous Province magmatism: tracing the extension of the Alpha Ridge onto Ellesmere Island, Canada. GSA Bull. 133 (7–8), 1695–1711. https://doi-org.ezproxy.uio.no/10.1130/B35792.1, 2020.
Park, J., Stein, H.J., Georgiev, S.V., Hannah, J.L., 2022. Degradation of Hg signals on incipient weathering: core versus outcrop geochemistry of Upper Permian shales, East Greenland and Mid-Norwegian Shelf. Chem. Geol. 608, 121030. https://doi.org/10.1016/j.chemgeo.2022.121030.
Percival, L.M.E., Witt, M.L.I., Mather, T.A., Hermoso, M., Jenkyns, H.C., Hesselbo, S.P., Al-Suwaidi, A.H., Storm, M.S., Xu, W., Ruhl, M., 2015. Globally enhanced mercury deposition during the end-Pliensbachian extinction and Toarcian OAE: a link to the Karoo–Ferrar Large Igneous Province. Earth Planet. Sci. Lett. 428, 267–280. https://doi.org/10.1016/j.epsl.2015.06.064.
Percival, L.M.E., Tedeschi, L.R., Creaser, R.A., Bottini, C., Erba, E., Giraud, F., Svensen, H., Savian, J., Trindade, R., Coccioni, R., Frontalini, F., Jovane, L., Mather, T.A., Jenkyns, H.C., 2021. Determining the style and provenance of magmatic activity during the Early Aptian Oceanic Anoxic Event (OAE 1a). Glob. Planet. Change 200, 103461. https://doi.org/10.1016/j.gloplacha.2021.103461.
Polteau, S., Hendriks, B.W.H., Planke, S., Ganerød, M., Corfu, F., Faleide, J.I., Midtkandal, I., Svensen, H., Myklebust, R., 2016. The Early Cretaceous Barents Sea sill complex: distribution, 40Ar/39Ar geochronology, and implications for carbon gas formation. Palaeogeogr. Palaeoclimatol. Palaeoecol. 441, 83–95.
Pyle, D.M., Mather, T.A., 2003. The importance of volcanic emissions for the global atmospheric mercury cycle. Atmos. Environ. 37 (36), 5115–5124.
Sanei, H., Grasby, S., Beauchamp, B., 2012. Latest Permian mercury anomalies. Geology 40, 63–66.
Schmidt, A., Skeffington, R.A., Thordarson, T., Self, S., Forster, P.M., Rap, A., Ridgwell, A., Fowler, D., Wilson, M., Mann, G.W., Wignall, P.B., Carslaw, K.S., 2015. Selective environmental stress from sulphur emitted by continental flood basalt eruptions. Nat. Geosci. 91 (9), 77–82. https://doi.org/10.1038/ngeo2588.
Senger, K., Buckley, S.J., Chevallier, L., Fagereng, Å., Galland, O., Kurz, T.H., Ogata, K., Planke, S., Tveranger, J., 2015. Fracturing of doleritic intrusions and associated contact zones: implications for fluid flow in volcanic basins. J. Afr. Earth Sci. 102, 70–85. https://doi.org/10.1016/j.jafrearsci.2014.10.019.
Shen, J., Algeo, T.J., Chen, J., Planavsky, N.J., Feng, Q., Yu, J., Liu, J., 2019. Mercury in marine Ordovician/Silurian boundary sections of South China is sulfide-hosted and non-volcanic in origin. Earth Planet. Sci. Lett. 511,p, 130–140. https://doi.org/10.1016/j.epsl.2019.01.028.
Shen, J., Feng, Q., Algeo, T.J., Liu, J., Zhou, C., Wei, W., Liu, J., Them, T.R., Gill, B.C., Chen, J., 2020. Sedimentary host phases of mercury (Hg) and implications for use of Hg as a volcanic proxy. Earth Planet. Sci. Lett. 543, 116333. https://doi.org/10.1016/j.epsl.2020.116333.
Shen, J., Yin, R., Algeo, T.J., Svensen, H.H., Schoepfer, S.D., 2022. Mercury evidence for combustion of organic-rich sediments during the end-Triassic crisis. Nat. Commun. 13, 1307. https://doi.org/10.1038/s41467-022-28891-8.
Snow, L.J., Duncan, R.A., Bralower, T.J., 2005. Trace element abundances in the Rock Canyon Anticline, Pueblo, Colorado, marine sedimentary section and their relationship to Caribbean plateau construction and oxygen anoxic event 2. Paleoceanography 20, PA3005. https://doi.org/10.1029/2004PA001093.
Svensen, H., Jamtveit, B., 1998. Contact metamorphism of shales and carbonates from the Grua area, the Oslo rift, Norway: a phase petrological study. Norwegian J. Geol. 78, 81–98.
Svensen, H., Corfu, F., Polteau, S., Hammer, O., Planke, S., 2012. Rapid magma emplacement in the Karoo Large Igneous Province. Earth Planet. Sci. Lett. 325, 1–9.
Svensen, H., Planke, S., Chevallier, L., Malthe-Sorenssen, A., Corfu, F., Jamtveit, B., 2007. Hydrothermal venting of greenhouse gases triggering Early Jurassic global warming. Earth Planet. Sci. Lett. 256 (3–4), 554–566.
Svensen, H., Planke, S., Malthe-Sorenssen, A., Jamtveit, B., Myklebust, R., Rasmussen Eidem, T., Rey, S.S., 2004. Release of methane from a volcanic basin as a mechanism for initial Eocene global warming. Nature 429 (6991), 542–545.
Svensen, H., Planke, S., Polozov, A.G., Schmidbauer, N., Corfu, F., Podladchikov, Y.Y., Jamtveit, B., 2009. Siberian gas venting and the end-Permian environmental crisis. Earth Planet. Sci. Lett. 277 (3–4), 490–500.
Svensen, H.H., Hammer, Ø, Chevallier, L., Jerram, D.A., Silkoset, P., Polteau, S., Planke, S., 2020. Understanding thermogenic degassing in Large Igneous Provinces: inferences from the geological and statistical characteristics of breccia pipes in the western parts of the Karoo Basin. In: Geological Society of America Books, Special Paper, vol. 544.
Svensen, H.H., Planke, S., Neumann, E.R., Aarnes, I., Marsh, J.S., Polteau, S., Harstad, C., Chevallier, L., 2015. Sub-volcanic intrusions and the link to global climatic and environmental changes. In: Breitkreuz, C., Rocchi, S. (Eds.), Physical Geology of Shallow Magmatic Systems. Advances in Volcanology. Springer.
Svensen, H., Polteau, S., Cawthorn, G., Planke, S., 2014. Sub-volcanic intrusions in the Karoo Basin. In: Breitkreuz, C., Rocchi, S. (Eds.), Physical Geology of Shallow Magmatic Systems. In: Advances in Volcanology. Springer.
Sweeney, J., Burnham, A.K., 1990. Evaluation of a simple model of vitrinite reflectance based on chemical kinetics, 536. AAPG Bulletin 74, 1559–1570.
Wu, Q., et al., 2021. High-precision U-Pb age constraints on the Permian floral turnovers, paleoclimate change, and tectonics of the North China block. Geology 49 (6), 677–681. https://doi-org.ezproxy.uio.no/10.1130/G48051.1.
Yallup, C., Edmonds, M., Turchyn, A.V., 2013. Sulfur degassing due to contact metamorphism during flood basalt eruptions. Geochim. Cosmochim. Acta 120, 263–279. https://doi.org/10.1016/j.gca.2013.06.025.
Zaputlyaeva, A., Mazzini, A., Blumenberg, M., Scheeder, G., Kürschner, W., Kus, J., Jones, M.T., Frieling, J., 2020. Recent magmatism drives hydrocarbon generation in north-east Java, Indonesia. Sci. Rep. 10, 1786.